quantitative reproducibility, the samples were placed into calibrated quartz capillary tubes permanently positioned in the resonance cavity.

[(Triphos)Rh(μ-S)$_2$Rh(triphos)](BPh$_4$)$_2$ (1). A mixture of [(C$_2$H$_4$)$_2$RhCl]$_2$ (0.07 g, 0.18 mmol) and AgBF$_4$ (0.07 g, 0.36 mmol) in THF (30 mL) was stirred for 1 h. After elimination of the precipitated AgCl, the filtrate was treated first with solid triphos (0.22 g, 0.36 mmol) and then with [(triphos)Rh(S$_2$CO)]BPh$_4$ (0.40 g, 0.35 mmol) in CH$_2$Cl$_2$ (20 mL). An immediate reaction occurred accompanied by carbon monoxide evolution. Brown crystals were formed following the addition of NaBPh$_4$ (0.14 g, 0.4 mmol) in ethanol (30 mL) and the slow evaporation of the solvent: yield 72%; Λ_M 103 cm^2 Ω^{-1} mol^{-1}. Anal. Calcd for C$_{130}$H$_{118}$B$_2$P$_6$Rh$_2$S$_2$: C, 72.36; H, 5.51; Rh, 9.53; S, 2.97. Found: C, 72.01; H, 5.65; Rh, 9.38; S, 2.83.

[(Triphos)Rh(μ-S)$_2$Co(triphos)](BPh$_4$)$_2$ (2). To azeotrope off the water of the perchlorate salt, a solution of Co(ClO$_4$)$_2$·6H$_2$O (0.13 g, 0.35 mmol) in *n*-butanol (100 mL) was gently concentrated by heating at boiling temperature to ca. 5 mL. Triphos (0.22 g, 0.35 mmol) in CH$_2$Cl$_2$ (10 mL) was then added. The resulting light orange solution was treated with [(triphos)Rh(S$_2$CO)]BPh$_4$ (0.4 g, 0.35 mmol) in CH$_2$Cl$_2$ (20 mL). As above carbon monoxide evolved. Addition of NaBPh$_4$ (0.14 g, 0.4 mmol) in ethanol (30 mL) and partial evaporation of the solvent under a slow stream of nitrogen gave brown crystals: yield 60%; Λ_M 98 cm^2 Ω^{-1} mol^{-1}. Anal. Calcd for C$_{130}$H$_{118}$B$_2$CoP$_6$RhS$_2$: C, 73.86; H, 5.62; Co, 2.78; Rh, 4.86; S, 3.03. Found: C, 73.21; H, 5.55; Co, 2.69; Rh, 4.77; S, 2.94. *Caution!* To avoid detonation of Co(ClO$_4$)$_2$, the solution must not be taken to near-dryness and solid material must not be allowed to deposit on the walls of the reaction flask. It is recommended that one work behind a protective barrier.

[(Triphos)Rh(μ-S)$_2$Pt(diphos)]BPh$_4$ (3). A solution of [(triphos)Rh(S$_2$CO)]BPh$_4$ (0.40 g, 0.35 mmol) in THF (20 mL) was added to a solution of (PPh$_3$)$_2$Pt(C$_2$H$_4$) (0.26 g, 0.35 mmol) in THF (10 mL). Immediately the color turned to deep red, and carbon monoxide evolved. Solid diphos (0.14 g, 0.35 mmol) was then added to the mixture, which was stirred for 15 min. Addition of NaBPh$_4$ (0.14 g, 0.4 mmol) in ethanol (30 mL) led to the precipitation of red crystals: 68%; Λ_M 41 cm^2 Ω^{-1} mol^{-1}. Anal. Calcd for C$_{91}$H$_{83}$BP$_5$PtRhS$_2$: C, 64.12; H, 4.90; Pt, 11.44; Rh, 6.03; S, 3.76. Found: C, 64.01; H, 4.85; Pt, 11.33; Rh, 5.98; S, 3.66.

[(Triphos)Rh(μ-S)$_2$Fe(CO)(etriphos)]BPh$_4$ (4). A solution of [(triphos)Rh(S$_2$CO)]BPh$_4$ (0.40 g, 0.35 mmol) in CH$_2$Cl$_2$ (20 mL) was added to a mixture of Fe(BF$_4$)$_2$·6H$_2$O (0.12 g, 0.35 mmol) in ethanol (10 mL) and etriphos (0.12 g, 0.35 mmol) in CH$_2$Cl$_2$ (20 mL) to give immediately a deep violet color. When the resulting solution was gently heated at 35 °C for 20 min, the color turned deep green. Upon addition of NaBPh$_4$ (0.14 g, 0.4 mmol) in ethanol (30 mL), green crystals were obtained: 73%; Λ_M 45 cm^2 Ω^{-1} mol^{-1}. Anal. Calcd for C$_{83}$H$_{98}$BFeOP$_6$RhS$_2$: C, 65.10; H, 6.45; Fe, 3.64; Rh, 6.72; S, 4.18. Found: C, 64.99; H, 6.41; Fe, 3.33; Rh, 6.58; S, 4.06.

[(Triphos)Rh(μ-S)$_2$Co(triphos)]BPh$_4$ (7). Method A. A mixture of [(C$_2$H$_4$)$_2$RhCl]$_2$ (0.07 g, 0.18 mmol) and AgBF$_4$ (0.07 g, 0.36 mmol) in THF (30 mL) was stirred for 1 h. After elimination of the precipitated AgCl, the filtrate was first treated with solid triphos (0.22 g, 0.36 mmol) and then with (triphos)Co(S$_2$CO) (0.27 g, 0.35 mmol) in CH$_2$Cl$_2$ (20 mL). An immediate reaction occurred accompanied by carbon monoxide evolution. Brown crystals were formed following the addition of NaBPh$_4$ (0.14 g, 0.4 mmol) in ethanol (30 mL) and the slow evaporation of the solvent; yield 62%.

Method B. NaBH$_4$ (10 mg, 0.26 mmol) in ethanol (10 mL) was added dropwise to a solution of **2** (0.32 g, 0.15 mmol) in CH$_2$Cl$_2$ (25 mL), which turned from orange-brown to red. Addition of ethanol (30 mL) and partial evaporation of the solvent under a fast stream of nitrogen gave red crystals: 35%; Λ_M 43 cm^2 Ω^{-1} mol^{-1}. Anal. Calcd for C$_{106}$H$_{98}$BCoP$_6$RhS$_2$: C, 70.94; H, 5.50; Co, 3.28; Rh, 5.73; S, 3.57. Found: C, 70.01; H, 5.55; Co, 3.27; Rh, 5.68; S, 3.43.

[(Triphos)Rh(μ-S)$_2$Rh(triphos)]BPh$_4$ (8). Method B reported above for **7** was successfully used for the preparation of this red compound except for substitution of **1** for **2**: yield 49%; Λ_M 45 cm^2 Ω^{-1} mol^{-1}. Anal. Calcd for C$_{106}$H$_{98}$BP$_6$Rh$_2$S$_2$: C, 69.24; H, 5.37; Rh, 11.19; S, 3.48. Found: C, 69.31; H, 5.24; Rh, 11.06; S, 3.43.

[(Triphos)Ni(μ-S)Ni(triphos)](BPh$_4$)$_2$ (9). A solution of [(triphos)Rh(S$_2$CO)]BPh$_4$ (0.40 g, 0.35 mmol) in CH$_2$Cl$_2$ (20 mL) was added to a mixture of Ni(BF$_4$)$_2$·6H$_2$O (0.12 g, 0.35 mmol) in ethanol (15 mL) and triphos (0.22 g, 0.35 mmol) in CH$_2$Cl$_2$ (20 mL). An immediate reaction occurred accompanied by carbon monoxide evolution. After the solution stood for 3 h, the originally formed dark brown color turned deep green. Green crystals were formed following the addition of NaBPh$_4$ (0.14 g, 0.4 mmol) in ethanol (30 mL) and the slow evaporation of the solvent; yield 15%.

Registry No. 1, 105139-43-3; **2**, 113686-46-7; **3**, 113686-48-9; **4**, 113686-50-3; **5**, 99955-64-3; **6**, 82590-72-5; **7**, 113686-52-5; **8**, 113686-54-7; **9**, 58593-52-5; (PPh$_3$)$_2$Pt(C$_2$H$_4$), 12120-15-9; [(C$_2$H$_4$)$_2$RhCl]$_2$, 12081-16-2; [(triphos)Co(μ-S)$_2$Co(triphos)]$^{2+}$, 73496-95-4; [(triphos)Co(μ-S)$_2$Co(triphos)]$^+$, 113686-57-0; [(triphos)Co(μ-S)$_2$Co(triphos)], 73770-23-7; [(triphos)Co(μ-S)$_2$Rh(triphos)], 113686-56-9; [(triphos)Rh(μ-S)$_2$Rh(triphos)], 113686-55-8; dithiocarbonic acid, 4741-30-4.

New Crystalline Phase of (Octaethylporphinato)nickel(II). Effects of π-π Interactions on Molecular Structure and Resonance Raman Spectra

Theodore D. Brennan,[1] W. Robert Scheidt,*[1] and John A. Shelnutt*[2]

Contribution from the Department of Chemistry, University of Notre Dame, Notre Dame, Indiana 46556, and Fuel Sciences Division, Sandia National Laboratories, Albuquerque, New Mexico 87185. *Received October 19, 1987*

Abstract: A new (third) crystalline phase of Ni(OEP) has been isolated and characterized by a single-crystal X-ray diffraction study and single-crystal resonance Raman spectroscopy. Single-crystal Raman measurements were also performed on the two previously described phases and the Raman spectra of the three phases compared. Differences in Raman spectra between the current new phase and the previously reported triclinic phase are interpreted in terms of π-π interactions found for this new phase. These spectral differences are also compared to solution Raman data that had been previously reported on aggregated and monomeric porphyrin derivatives. The bands most affected are the core-size marker bands ν_{10}, ν_{19}, and ν_3 and the oxidation-state marker band ν_4 where π-π interaction leads to increases of 2.5-4.3 cm^{-1}. These Raman shifts are consistent with a decrease in the core size, and the crystal structure confirms this interpretation. The two crystallographically distinct Ni-N bond distances in the new crystalline phase are 1.946 (4) and 1.958 (4) Å, with the shorter distance along the one-dimensional stack axis of the complex. The observed interplanar spacing between porphyrin planes is 3.44 Å, and the Ni···Ni separation is 4.80 Å. Crystal data: triclinic; space group $P\bar{1}$; a = 13.302 (6), b = 13.342 (11), c = 4.802 (2) Å; α = 92.21 (2), β = 93.52 (4), γ = 113.43 (6)°; Z = 1; V = 778.7 Å^3. A total of 2568 unique observed data to a maximum (sin θ)/λ of 0.726 was used in the structure solution and refinement.

Meyer[3] and Cullen and Meyer[4] have reported the crystal and molecular structure of two different crystalline phases of four-coordinate (2,3,7,8,11,12,17,18-octaethylporphinato)nickel(II), Ni(OEP).[5] An important feature of these two crystalline phases

0002-7863/88/1510-3919$01.50/0

of Ni(OEP) is distinctly different porphinato core conformations. As pointed out by Hoard,[6] these core conformations are responsible for the substantial differences in the Ni–N bond lengths in the two crystalline forms. Thus, the ruffled tetragonal form[3] has a Ni–N bond distance of 1.929 (3) Å, fully 0.03 Å shorter than that found for the planar, triclinic form.[4] Hence, these studies led to the now well-recognized effects of porphinato core conformation on the M–N bond lengths. In a classic Raman study,[7] Spaulding et al. showed that there are a number of structure-sensitive Raman marker lines of metalloporphyrins that can be used to deduce the geometric parameters of the derivative. Important data in this Raman study were obtained from two different Ni(OEP) solids: One was clearly the tetragonal phase, and the second was called triclinic. However, it was probably not the triclinic phase described by Cullen and Meyer[4] but another distinct crystalline phase. Nickel porphyrinates were used by Kitagawa and co-workers[8] in their normal-mode assignments for porphinato derivatives.

These studies, taken as a group, have had a significant influence on our development of understanding metalloporphyrin structure and bonding even though the compounds are relatively simple porphyrin derivatives.

In the course of other work with Ni(OEP), we have obtained a third crystalline form of the four-coordinate species. Since the two previously investigated phases, taken as a group, were extremely illuminating, we expected that this third phase would also be worthy of investigation. Accordingly, we have determined the crystal and molecular structure of this third phase by an X-ray diffraction study. This species has a solid-state environment that is distinct from that reported for the other two crystalline phases, namely an extended π–π stacking of individual Ni(OEP) molecules. We report in this paper the effects of the π–π interaction on the structure of the Ni(OEP) molecule. We have used resonance Raman spectroscopy to investigate the effects of stacking in these different square-planar crystalline forms of Ni(OEP) and compare the Raman results for crystalline and solution aggregates. We find similarities between the monomer–dimer spectral differences in solution and those in the crystals. For example, the increase in frequency in the core-size marker lines for both crystal and solution "aggregates" relative to the "monomer" forms predict a contraction of the central core, and, indeed, the X-ray crystal structure shows the contraction occurs in the case of the crystal aggregates. Finally, we have investigated the question of why different crystalline phases of Ni(OEP) have been isolated. We distinguish our new crystalline form, which crystallizes in the triclinic crystal system, from the original triclinic form reported by Cullen and Meyer[4] by denoting them as triclinic B and triclinic A, respectively.

Experimental Section

Raman Spectra. All Raman spectra were obtained with a Raman difference spectrometer described previously.[9] For single-crystal Raman spectra the difference spectrometer was used in the conventional mode; therefore, for accurate determination of frequencies, several spectra of each crystalline form were required. As an example, eight spectra of each triclinic form were collected. Peak positions for the Raman lines were determined from the fast Fourier transform smoothed spectra, and average peak frequencies and probable errors were determined.

Typically, the Raman spectra were obtained with less than 10 mW of the 501.7-nm radiation from an argon ion laser impinging at a grazing incidence on a single crystal of Ni(OEP). In some cases the 413.1-nm line of a krypton ion laser was used. Much of the incident light is reflected from the shiny facet of the crystal so that the absorbed light is ≤1 mW. At much higher light power, the crystal could be sublimed as a violet vapor. No sample heating was evident at the lower power levels used in this study.

Scattered light was collected at 90° to the direction of propagation and polarization of the exciting laser light. Each of the Raman spectra consists of about 10 20-min scans of a 400-cm^{-1} region of the spectrum. Spectral resolution is 5 cm^{-1}. No change in the Ni(OEP) spectrum was noted during signal averaging, and no change was observed in the surface of the crystal when examined under a microscope at the end of data collection.

Table I. Fractional Coordinates [Ni(OEP)][a]

atom	x	y	z
Ni	0.0000	0.0000	0.0000
N(1)	0.0601 (3)	−0.0655 (3)	0.2847 (8)
N(2)	0.1282 (3)	0.1388 (3)	0.0772 (8)
C(1)	0.0169 (4)	−0.1723 (4)	0.3667 (11)
C(2)	0.0888 (5)	−0.1887 (5)	0.5762 (11)
C(3)	0.1746 (5)	−0.0934 (5)	0.6344 (11)
C(4)	0.1578 (4)	−0.0156 (4)	0.4550 (11)
C(5)	0.2293 (4)	0.0901 (5)	0.4475 (11)
C(6)	0.2176 (4)	0.1623 (4)	0.2652 (11)
C(7)	0.2970 (5)	0.2734 (4)	0.2510 (12)
C(8)	0.2553 (4)	0.3179 (5)	0.0570 (13)
C(9)	0.1492 (4)	0.2352 (4)	−0.0532 (11)
C(10)	0.0821 (5)	0.2501 (4)	−0.2565 (12)
C(11)	0.0694 (5)	−0.2968 (5)	0.7030 (13)
C(12)	0.1157 (7)	−0.3634 (6)	0.5356 (18)
C(13)	0.2729 (5)	−0.0673 (5)	0.8404 (12)
C(14)	0.3693 (6)	−0.0750 (8)	0.7015 (19)
C(15)	0.4062 (5)	0.3206 (5)	0.4157 (14)
C(16)	0.4908 (6)	0.2808 (6)	0.2964 (18)
C(17)	0.3031 (5)	0.4327 (5)	−0.0330 (13)
C(18)	0.2574 (6)	0.5075 (5)	0.1147 (15)

[a] The estimated standard deviations of the least significant digits are given in parentheses.

Structure Determination. A satisfactory crystal of the triclinic B phase was obtained by slow evaporation of a methylene chloride solution of Ni(OEP). The crystal used for data collection was a segment 0.51 × 0.08 × 0.08 mm cut from a longer dark purple needle. The crystal was mounted with the long axis roughly along the ϕ axis of the goniometer. All preliminary examination and intensity data collection were done on an Enraf-Nonius CAD4 diffractometer using graphite-monochromated Mo Kα radiation ($\bar{\lambda}$ = 0.71073 Å). Cell constants were determined from a least-squares refinement of the setting angles of 25 reflections in the range $20 < 2\theta < 28°$. Triclinic cell parameters were found to be a = 13.302 (6) Å, b = 13.342 (11) Å, c = 4.802 (2) Å, α = 92.21 (2)°, β = 93.52 (4)°, γ = 113.43 (6)°, Z = 1, and V = 778.7 Å^3. The calculated and observed crystal densities were 1.26 g/cm^3. A Delauney reduction did not reveal any hidden symmetry. The space group was initially assumed to be the centrosymmetric choice $P\bar{1}$. This choice was confirmed by all subsequent developments during structure solution and refinement. Data were collected at ambient conditions (21 ± 1 °C) by θ–2θ scans to a maximum $(\sin\theta)/\lambda$ of 0.726. Two equivalent sets of reflections were measured, leading to a total of 9813 $\pm h,\pm k,\pm l$ reflections. Of these, 4908 are unique and 2568 were considered observed following the criterion of $F > 3\sigma F$. For the observed data averaged, the agreement factors were 2.7% on I and 2.6% on F. Four standard reflections, measured every 1 h showed no decay over the 117 h of data collection. Data were corrected for Lorentz and polarization effects but not for absorption.

The symmetry of the space group requires that the nickel(II) ion be placed on an inversion center; the remainder of the molecule was located in a subsequent difference Fourier map.[10] Least-squares refinement was eventually carried to convergence with anisotropic thermal parameters for all heavy atoms and idealized hydrogen atom positions (C–H = 0.95 Å). Refinement converged at R_1 = 0.066 and R_2 = 0.083 and an error of fit of 2.86. The final difference Fourier was judged to be essentially

(1) University of Notre Dame.
(2) Sandia National Laboratories.
(3) Meyer, E. F., Jr. *Acta Crystallogr., Sect. B: Struct. Crystallogr. Cryst. Chem.* **1972**, *B28*, 2162.
(4) Cullen, D. L.; Meyer, E. F., Jr. *J. Am. Chem. Soc.* **1974**, *96*, 2095.
(5) Abbreviations used: OEP, dianion of 2,3,7,8,11,12,17,18-octaethylporphyrin; TMP, dianion of 5,10,15,20-tetramethylporphyrin; TPrP, dianion of 5,10,15,20-tetrapropylporphyrin; UroP, dianion of uroporphyrin.
(6) Hoard, J. L. *Ann. N.Y. Acad. Sci.* **1973**, *206*, 18.
(7) Spaulding, L. D.; Chang, C. C.; Yu, N.-T.; Felton, R. H. *J. Am. Chem. Soc.* **1975**, *97*, 2517.
(8) Kitagawa, T.; Abe, M.; Ogoshi, H. *J. Chem. Phys.* **1978**, *69*, 4516. Abe, M.; Kitagawa, T.; Kyogku, Y. *J. Chem. Phys.* **1978**, *69*, 4526.
(9) Shelnutt, J. A. *J. Phys. Chem.* **1983**, *87*, 605.
(10) Programs used in this study included local modifications of Jacobson's ALLS, Zalkin's FORDAP, Busing and Levy's ORFFE and ORFLS, and Johnson's ORTEP2. Atomic form factors were from: Cromer, D. T.; Mann, J. B. *Acta Crystallogr., Sect. A: Cryst. Phys., Diffr., Theor. Gen. Crystallogr.* **1968**, *A24*, 321. Real and imaginary corrections for anomalous dispersion in the form factor of the nickel atom were from: Cromer, D. T.; Liberman, D. J. *J. Chem. Phys.* **1970**, *53*, 1891. Scattering factors for hydrogen were from: Stewart, R. F.; Davidson, E. R.; Simpson, W. T. *Ibid.* **1965**, *42*, 3175. All calculations were performed on a VAX 11/730.

Table II. Frequencies (and Probable Errors)[a] of Structure-Sensitive Raman Marker Lines of Nickel Octaethylporphyrin Crystals and Differences (Δ) between the Two Triclinic Forms

assignt[b]	triclinic A	triclinic B	Δ(B−A)	tetragonal
ν_{10}	1659.0 (1.4)	1662.2 (1.0)	3.2	1641
ν_{19}	1605.5 (1.1)	1608.4 (1.0)	2.9	1595
ν_{11}	1580.3 (1.4)	1579.5 (1.1)	−0.8	1573
ν_3	1520.5 (0.9)	1524.8 (0.7)	4.3	1514
ν_{29}	1405.9 (0.9)	1407.2 (0.8)	1.3	1405
ν_4	1380.4 (1.0)	1382.9 (0.9)	2.5	1383
ν_{21}	1306.3 (0.2)	1307.5 (0.7)	1.2	1299
	1257			
ν_{13}	1215			
ν_{30}	1155			
	1134			
ν_5	1023			
	1120			
	1110			
	960			
	840			
ν_6	801			
	765			
ν_{16}	748			
ν_7	671			
ν_8	342	354	12	345
		320		
	276	276	0	279
	218	235	17	246

[a] Probable error 0.6745σ. [b] Assignments are taken from ref 8.

featureless; the largest peak had a height of 0.66 e/Å^3 and was located near the nickel atom. Final tables of atomic coordinates are given in Table I. Final anisotropic temperature factors are listed in Table SI of the supplementary material.

Crystallization Experiments. The initial experiment that led to the isolation of the new (triclinic B) crystalline form of Ni(OEP) was the slow evaporation of a saturated methylene chloride solution containing about 20% pyridine. Ni(OEP) was obtained from Aldrich Chemical Co. Subsequent crystallization experiments were slow evaporation of either methylene chloride or carbon tetrachloride/methylene chloride solutions. In all original crystallization experiments, mixtures of two or even all three crystalline forms of Ni(OEP) were obtained. The various individual phases are distinguishable on the basis of crystal morphology. Assignments of phase were also confirmed by X-ray diffraction measurements used to determine unit cell constants. The tetragonal phase is readily identified by the formation of tetragonal bipyramids. The original triclinic phase (triclinic A) is readily distinguishable from the new triclinic phase (triclinic B) in that crystals of the former (A) are well-defined prisms while the B phase are found as long needles. The original Ni(OEP) samples used for crystal preparation were found to contain a small (~3%) amount of free base H_2OEP.[11] An increased concentration of H_2OEP in the crystalline triclinic A form compared to the triclinic B form was suggested from the impurity signal level in the resonance Raman spectrum. H_2OEP was removed by column chromatography on silica gel with carbon tetrachloride as eluent. Subsequent crystallization experiments used these purified samples of Ni(OEP) as well as "synthetically" impure samples of Ni(OEP) prepared by the addition of 3% H_2OEP (by weight).

Results

Raman Spectra. Figure 1 shows typical Raman spectra of the three crystalline forms of Ni(OEP) and, for comparison, the spectrum of crystalline H_2OEP known to be isomorphous with the triclinic A Ni(OEP) phase. Raman spectra of an unknown phase (actually probably that of triclinic B from a description of crystals) and the tetragonal phase were reported previously.[7]

H_2OEP appears to be an impurity in the Ni(OEP) crystals whose spectra are shown in Figure 1. The apparent amount of H_2OEP present in the crystals is exaggerated by preferential resonance enhancement at the excitation wavelength employed. Selective enhancement of the impurity results from resonance of the 501.7-nm laser radiation with the strong vibronic sideband of the Q_y transition of H_2OEP;[12] the exciting light is farther from resonance with any Ni(OEP) absorption bands. When Ni(OEP) with no detectable free-base impurity was crystallized, the Raman lines of H_2OEP disappear in the single-crystal Raman spectra. Also, when crystals showing the putative free-base impurity were dissolved in methylene chloride, initial scans of the Raman spectra show lines of H_2OEP, but these Raman lines rapidly disappear as the impurity photodecomposes. Photodecomposition in solution is also consistent with the impurity being the free base. Slow photodecomposition of the H_2OEP impurity is also noted in the crystals.

Table II lists frequencies of the major Ni(OEP) Raman lines. Assignments are those of Kitagawa and co-workers.[8] Some large-frequency differences occur for lines in the 200–400-cm^{-1} region for the two triclinic crystals, but we focus on the high-frequency marker lines in the 1300–1700-cm^{-1} region of the Raman spectra in the present work. When the triclinic A and B forms are compared, small but significant differences in frequency of the core-size markers[7,13] ν_{10}, ν_{19}, and ν_3 are noted. These lines are higher by 2.9–4.3 cm^{-1} for the triclinic form with the small lateral shift (form B). The core-size marker lines are also sensitive to oxidation state and π charge density in the macrocycle.[13-16] Significantly, the oxidation-state marker line ν_4 also increases by 2.5 cm^{-1} for the triclinic B crystal. Other shifts of about 1 cm^{-1} to high or low frequency are observed for ν_{21}, ν_{29}, and ν_{11}. ν_{11} is known to be at most only weakly dependent on core size.[13]

Much larger differences are apparent when either of the triclinic forms are compared with the tetragonal form of Ni(OEP).[7] In

Table III. Bond Distances in [Ni(OEP)]

	dist, Å		dist, Å
Ni–N(1)	1.946 (4)	C(1)–C(2)	1.429 (7)
Ni–N(2)	1.958 (4)	C(4)–C(3)	1.449 (8)
N(1)–C(1)	1.391 (6)	C(6)–C(7)	1.445 (8)
N(1)–C(4)	1.392 (6)	C(9)–C(8)	1.454 (7)
N(2)–C(6)	1.372 (6)	C(2)–C(11)	1.520 (8)
N(2)–C(9)	1.386 (6)	C(3)–C(13)	1.504 (8)
C(1)–C(10)′	1.369 (8)	C(7)–C(15)	1.492 (8)
C(4)–C(5)	1.355 (8)	C(8)–C(17)	1.499 (8)
C(5)–C(6)	1.373 (8)	C(11)–C(12)	1.502 (9)
C(9)–C(10)	1.356 (8)	C(13)–C(14)	1.518 (9)
C(2)–C(3)	1.333 (8)	C(15)–C(16)	1.552 (9)
C(7)–C(8)	1.330 (8)	C(17)–C(18)	1.533 (9)

Table IV. Bond Angles in [Ni(OEP)]

	angle, deg		angle, deg
N(1)–Ni–N(2)	89.9 (2)	C(6)–C(7)–C(8)	106.6 (5)
C(1)–N(1)–C(4)	103.5 (4)	C(9)–C(8)–C(7)	107.6 (5)
C(6)–N(2)–C(9)	104.6 (4)	C(4)–C(3)–C(2)	106.9 (5)
C(1)–N(1)–Ni	128.7 (4)	C(1)–C(2)–C(3)	107.7 (5)
C(4)–N(1)–Ni	127.8 (4)	C(2)–C(11)–C(12)	111.5 (5)
C(6)–N(2)–Ni	128.3 (4)	C(3)–C(13)–C(14)	111.7 (5)
C(9)–N(2)–Ni	127.0 (3)	C(7)–C(15)–C(16)	112.9 (5)
N(1)–C(1)–C(10)′	123.3 (5)	C(8)–C(17)–C(18)	112.6 (5)
N(1)–C(4)–C(5)	124.7 (5)	C(1)–C(2)–C(11)	125.1 (5)
N(2)–C(6)–C(5)	124.3 (5)	C(4)–C(3)–C(13)	124.6 (5)
N(2)–C(9)–C(10)	125.3 (5)	C(6)–C(7)–C(15)	123.9 (5)
N(1)–C(1)–C(2)	111.2 (5)	C(9)–C(8)–C(17)	124.2 (5)
N(1)–C(4)–C(3)	110.7 (5)	C(3)–C(2)–C(11)	127.2 (5)
N(2)–C(6)–C(7)	111.4 (5)	C(2)–C(3)–C(13)	128.6 (6)
N(2)–C(9)–C(8)	109.8 (5)	C(8)–C(7)–C(15)	129.3 (5)
C(4)–C(5)–C(6)	124.9 (5)	C(7)–C(8)–C(17)	128.2 (5)
C(9)–C(10)–C(1)	125.5 (5)	C(5)–C(6)–C(7)	124.4 (5)
C(10)–C(1)–C(2)	125.5 (5)	C(10)–C(9)–C(8)	124.8 (5)
C(5)–C(4)–C(3)	124.6 (5)		

(11) The H_2OEP impurity is readily detectable by thin-layer chromatography on silica gel plates. The impurity is less readily detectable by UV–vis spectroscopy. Ni(OEP) is specified as 97% by Aldrich; the impurities are not specified.

(12) Gouterman, M. In *The Porphyrins*; Dolphin, D., Ed.; Academic: New York, 1978; Chapter 1.

(13) Spiro, T. G. In *Iron Porphyrins*; Lever, A. B. P., Gray, H. B., Eds.; Addison-Wesley: Reading, MA, 1982; Part II, Chapter 2.

(14) Yamamoto, T.; Palmer, G.; Salmeen, I. T.; Rimai, L. *J. Biol. Chem.* **1973**, *248*, 5211.

(15) Spiro, T. G.; Strekas, T. C. *J. Am. Chem. Soc.* **1974**, *96*, 338.

(16) Spiro, T. G.; Burke, J. M. *J. Am. Chem. Soc.* **1976**, *98*, 5482.

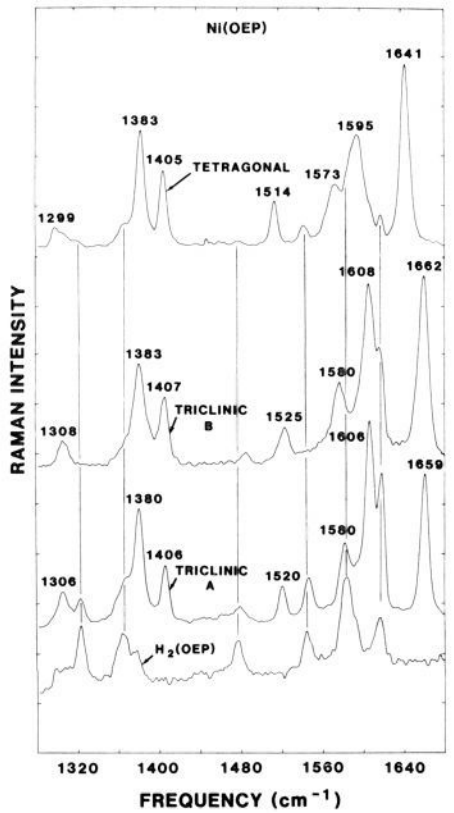

Figure 1. Typical Raman spectra for the three crystalline forms of Ni(OEP) and crystalline H_2OEP in the 1300–1680-cm^{-1} region.

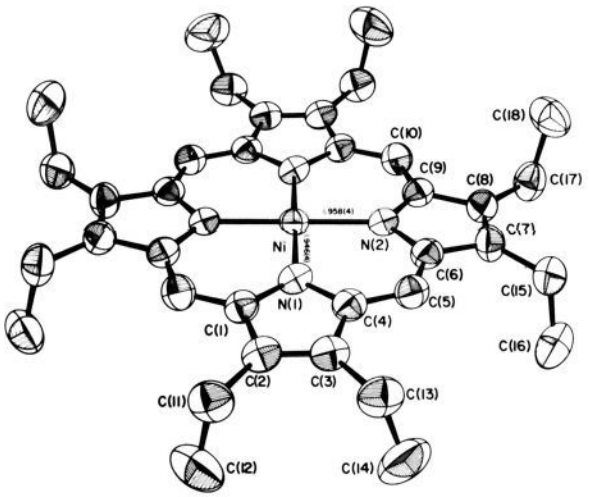

Figure 2. ORTEP diagram of the Ni(OEP) molecule as it exists in the triclinic B phase. Atoms are contoured at the 50% probability level. The atom labels for the crystallographically unique atoms of the molecule are displayed.

particular, for the tetragonal form, core-size marker lines are from 7 to 21 cm^{-1} lower than those for the triclinic crystals (see Table II). These large differences are thought to result from ruffling of the macrocycle rather than the core expansion predicted by the empirical correlation existing between core-size and marker-line frequency that has been found for the metalloporphyrins with near-planar configurations.[7,13]

Structure Determination. The molecular structure of the triclinic B form of Ni(OEP), is displayed in Figure 2, which also gives the atom labels for the crystallographically unique half of the Ni(OEP) molecule as it exists in the crystal. The molecule has a crystallographically required inversion center at the nickel atom. Individual values of bond distances and bond angles for the

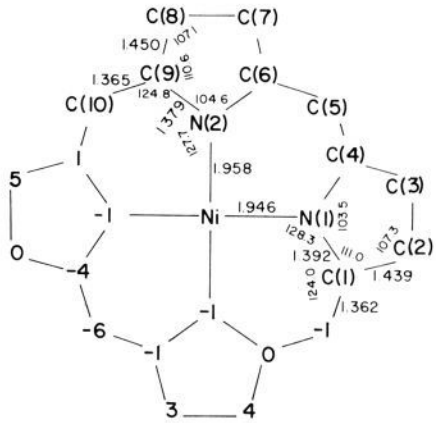

Figure 3. Formal diagram of a porphinato core displaying the displacements of the crystallographically unique atoms, in units of 0.01 Å, from the mean plane of the 24-atom porphinato core.

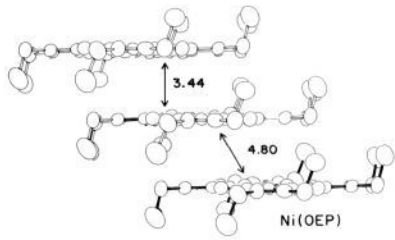

Figure 4. Edge-on view of the Ni(OEP) π–π aggregate in the triclinic B phase. Distances shown are the Ni···Ni separation and the mean plane separation, which are repeated indefinitely along the chain.

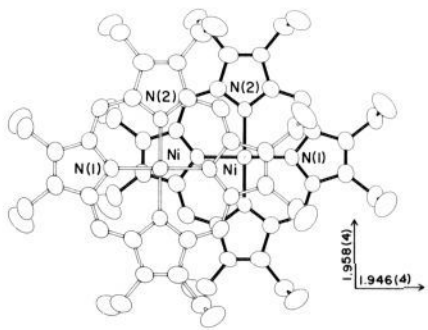

Figure 5. Overlap diagram showing two of the interacting Ni(OEP) units displayed in Figure 4.

molecule are tabulated in Tables III and IV, respectively. Figure 3 displays the deviation of the crystallographically unique individual atoms, in units of 0.01 Å, from the mean plane of the 24-atom core. As can be seen from the figure, the deviation from exact planarity is unremarkable. The average Ni–N distance of 1.952 (8) Å is slightly shorter than the 1.96-Å values observed previously[4,17] for nickel derivatives with planar porphyrin cores; the variation in the values of Ni–N in this new form of Ni(OEP) commands subsequent attention. No other features of the molecular structure are unexpected for nickel(II) species.

Figures 4 and 5 display features of the π–π interaction between Ni(OEP) molecules. The molecules form an extended one-dimensional symmetric aggregate along the c axis. Figure 4 is an edge-on view of three molecules of the extended aggregate. As shown in the diagram, nickel(II) ions are separated by the cell translation of 4.80 Å, and the separation between adjacent mean planes of the porphinato core is 3.44 Å. Figure 5 is a view of two Ni(OEP) units in a direction perpendicular to that of Figure 4 that shows the relative overlap of the porphyrin cores in the aggregate. The crystallographic symmetry between molecules in

(17) Hamor, T. A.; Caughey, W. S.; Hoard, J. L. *J. Am. Chem. Soc.* **1965**, *87*, 2305.

Table V. Comparison of Averaged Bond Lengths (Å) and Angles (deg) in the Three Crystalline Forms of Ni(OEP)

	tri-B ring 1		tri-B ring 2	tri-A	tetrag
Ni–N	1.946 (4)		1.958 (4)	1.958 (2)	1.929 (3)
C_a–N	1.392 (1)		1.379 (10)	1.376 (6)	1.386 (2)
C_a–C_m	1.362 (10)		1.365 (12)	1.371 (4)	1.372 (1)
C_a–C_b	1.439 (14)		1.450 (6)	1.443 (3)	1.449 (5)
C_b–C_b	1.333 (8)		1.330 (8)	1.346 (2)	1.362 (5)
Ni–C_a	3.012 (8)		3.006 (2)	3.006 (4)	2.983 (1)
Ni–C_m		3.382 (1)		3.381 (1)	3.355 (4)
N–Ni–N		90.1 (2)		90.15 (9)	90.0
Ni–N–C_a	128.3 (6)		127.7 (9)	128.0 (2)	127.4 (2)
C_a–N–C_a	103.5 (4)		104.6 (4)	103.9 (4)	105.1 (3)
N–C_a–C_m	124.0 (10)		124.8 (7)	124.4 (3)	124.0 (2)
N–C_a–C_b	111.0 (4)		110.6 (11)	111.6 (3)	110.6 (2)
C_m–C_a–C_b	125.0 (6)		124.6 (3)	124.1 (4)	125.0 (2)
C_a–C_b–C_b	107.3 (6)		107.1 (7)	106.5 (4)	106.8 (3)
C_a–C_m–C_a		125.2 (4)		125.1 (2)	124.1 (2)
required symmetry		C_i		C_i	S_4
ref		this work		4	3

the crystal leads to exactly parallel porphinato planes in the aggregate stack illustrated in Figures 4 and 5. A final geometric parameter is the lateral shift, which we have described and used elsewhere[18] in a compilation of geometry for π–π interactions in porphyrin species. The lateral shift is the separation between the centers of pairs of cores, measured in the direction parallel to the mean plane. In the triclinic B phase, the lateral shift is 3.35 Å. The intermolecular interactions of the triclinic A phase of Ni(OEP) are much weaker as measured by these geometric parameters. In phase A, Ni(OEP) molecules interact in pairs with an interplanar separation of 3.48 Å but with a Ni···Ni separation of 7.62 Å and a lateral shift of 6.78 Å. The corresponding distances are larger still in the tetragonal phase. These π–π geometric parameters place the triclinic B phase in the group we have called[18] the "intermediate" group while those in the other Ni(OEP) phases place them in the "weak" group.

Crystallization Experiments. All original samples of Ni(OEP) yielded mixtures of at least two distinct crystalline phases, with triclinic A almost always observed. However, crystallization experiments that were performed with pure samples of Ni(OEP) yielded very little if any[19] of the triclinic phase A. Rather, the crystals from such pure samples of Ni(OEP) were varying proportions of the tetragonal phase and triclinic B. However, readdition of H_2OEP to the crystallization solution led to the reappearance of the triclinic A phase.

Discussion

Molecular Structure. The determination of structure for this triclinic B phase of Ni(OEP) with its π–π interactions in the solid state allows us to examine an interesting question, namely whether these interactions have an effect on the Ni(OEP) molecular structure. The available evidence suggests a real effect. As shown in Figure 5, the π–π overlap between porphinato cores in the extended aggregate involves two (trans) pyrrole rings to a much larger extent than the other pyrrole rings. The pyrrole rings more extensively involved in the between-core interactions also have the shorter Ni–N bonds (1.946 (4) Å vs 1.958 (4) Å). Additionally, the shorter N–C_a bond lengths and the smaller C_a–N–C_a bond angle in the pyrrole ring with the shorter Ni–N bond distance are in accord with expectation[6] if there were real differences in the Ni–N bond lengths. Average values for all bond parameters of the two distinct pyrrole rings are shown in Figure 3. In Table V, the average bond parameters are compared with the values found for the two other crystalline forms of Ni(OEP). Also listed in Table V are the porphinato core conformation of each crystalline form. It should be recalled[6] that core conformations can have significant effects on bond parameters. Thus, the strongly ruffled tetragonal form of Ni(OEP) is not as directly comparable with the new triclinic B form as that of the triclinic A form. Both triclinic forms have planar cores and, as can be seen in Table V, the bond parameters of two forms are similar. This is especially true for the parameters of ring 2 of triclinic B and the averaged parameters of triclinic A, which have identical Ni–N bond lengths.

Additional confirming evidence for π–π interactions having a significant effect on the geometry comes from the structure[20] of Fe(OEP). Crystalline Fe(OEP) is isomorphous with the triclinic B form of Ni(OEP) and hence has a quite similar molecular environment in the solid state. For Fe(OEP), the two Fe–N distances are 1.984 (5) and 2.007 (5) Å and the shorter distance involves the pyrrole ring with the extensive overlap in the π–π aggregate. Differences in bond parameters for the two unique pyrrole rings also follow the same pattern as that of the triclinic B form of Ni(OEP). Although the precision of iron structure is no better than that of Ni(OEP), the pattern of deviations strongly suggests the importance of π–π interactions on the solid-state structure of both compounds. Ibers[21] and co-workers have also observed a similar linear stack in Ni(TMP). In Ni(TMP), nonequal Ni–N distances of 1.943 (1) and 1.963 (1) Å are observed, with the shorter distance again involving the pyrrole ring having the more significant π–π overlap. A combination theoretical and experimental bonding electron density study[21b] was interpreted as suggesting that the perturbation engendered by the stack is too small to explain the observed geometric distortion.

The common occurrence of nonequivalent M–N bond distances in the above one-dimensional aggregate stacks led us to question whether this was a general feature of metalloporphyrin structure. Since Scheidt and Lee[18] have summarized geometric parameters for porphyrin derivatives involving π–π interactions in the solid, finding all known examples was straightforward. There is only one additional example of an aggregate structure of this type. It is exhibited by Cu(TPrP).[22] Curiously, again the short Cu–N distance (1.994 Å vs 2.005 Å) is in the direction of the extended π–π stack. It is to be noted that the differences in Cu–N bond distance are not statistically significant, but the continued occurrence of the pattern commands attention.

Raman Results. The most important result of the Raman investigation is that structurally dependent changes found in the triclinic B crystal form are similar to those occurring upon porphyrin aggregation in solution. The frequency differences found for triclinic A ("monomer crystal packing") and triclinic B ("aggregate crystal packing") lead us to expect (i) a slight contraction of the porphinato core and (ii) a small decrease in the π charge density in the ring. Core contraction of between 0.006 and 0.010 Å is expected based on the increase in frequency for the core-size marker lines ν_3, ν_{19}, and ν_{10} (assuming 0.0022-, 0.0020-, and 0.0019-Å contraction per wavenumber shift).[13] Indeed a contraction of 0.006 Å is found in the average Ni–N bond distance in triclinic B compared to triclinic A.

The conclusion that the π charge density in the ring decreases upon π–π aggregation in the crystal is on a weaker footing. This interpretation is based on studies[13-16] showing that a number of Raman lines including ν_{21}, ν_4, ν_3, ν_{19}, and ν_{10} increase proportionately with a decrease in the π charge density in the π^* orbitals of the porphyrin. The result is based on the dependence of the frequency of these lines on oxidation state[15] and axial ligand basicity[16] for iron porphyrins and on π anion formation[23] for vanadyl and zinc porphyrinates. Although the results may not

(18) Scheidt, W. R.; Lee, Y. J. *Struct. Bonding (Berlin)* **1987**, *64*, 1–70.

(19) In the crystallization experiments with pure Ni(OEP), no crystals large enough for a diffraction measurement were found that could have been considered a sample of the triclinic A phase (i.e., all large crystals are either triclinic B or tetragonal). There remains the possibility that some of the *microcrystalline* material is the triclinic A phase.

(20) Straus, S. H.; Silver, M. E.; Long, K. M.; Thompson, R. G.; Hudgens, R. A.; Spartalian, K.; Ibers, J. A. *J. Am. Chem. Soc.* **1985**, *107*, 4207.

(21) (a) Gallucci, J. C.; Sweptson, P. N.; Ibers, J. A. *Acta Crystallogr., Sect. B: Struct. Crystallogr. Cryst. Chem.* **1982**, *B38*, 2134. (b) Kutzler, F. W.; Sweptson, P. N.; Berkovitch-Yellin, Z.; Ellis, D. E.; Ibers, J. A. *J. Am. Chem. Soc.* **1983**, *105*, 2996.

(22) Moustakali, I.; Tulinsky, A. *J. Am. Chem. Soc.* **1973**, *95*, 6811.

(23) Ksenofontova, N. M.; Maslov, V. G.; Sidorov, A. N. Bobovich, Ya. S. *Opt. Spectrosc. (Engl. Transl.)* **1976**, *40*, 462.

carry over to the nickel porphyrinates, the combined X-ray and Raman results are suggestive. A contraction of the ring would be expected because the charge density in π^* orbitals of the ring decreases; the decrease would result in a general strengthening and shortening of some macrocyclic skeletal bonds. As noted earlier, the N–C_a bonds of the pyrrole ring most involved in the π–π interaction are shortened.

The triclinic crystal Raman results mimic well the results previously obtained from solution studies of π–π aggregation. The metallouroporphyrins have provided a novel means of investigating aggregation phenomena in solution.[9,24-26] The uroporphyrins are monomeric in aqueous base below 1×10^{-3} M because of their high peripheral charge (−8), but under acid or high ionic strength (>1 M) conditions, the charge is shielded and the uroporphyrin aggregates or dimerizes. For example, Ni(UroP) at 1×10^{-4} M dimerizes at 5.5 M salt as evidenced by a 13-nm blue shift in the Soret band and a 3-nm red shift in the α band.[24]

In contrast with the large effect of dimerization on the absorption spectrum, only small shifts are found in the Raman marker lines. For example, the salt-induced shifts in ν_4, ν_3, ν_{19}, and ν_{10} for Ni(UroP) are 0.7, 2.9, 2.7, and 1.6 cm^{-1}.[24] The shifts compare with 2.5, 4.3, 2.9, and 3.2 cm^{-1} for the triclinic B–A differences (Table II). Thus, aggregation in the crystal causes shifts in the core-size markers of similar magnitude (1–3 cm^{-1}) and direction (an increase) as for the solution aggregates. The same general pattern of marker line shifts is observed for formation of Cu-, Fe(OH)-, Pt-, and Pd(UroP) salt dimers. One difference in solution and crystal π–π aggregation behavior is evident in the salt-induced shifts in ν_{21}. However, the vibrational mode ν_{21} is known to be sensitive to the nature and orientation of peripheral substituents.[13,27]

Other kinds of π–π intermolecular interactions give similar Raman results. As a first example, formation of aqueous π–π complexes with neutral aromatic acceptors such as phenanthroline gives a stacked complex, with one or two phenanthroline molecules occupying the faces of the porphyrin ring.[9,28] For metalloporphyrins that are four-coordinate, both top and bottom faces are occupied by phenanthroline molecules. When the metalloporphyrin is five-coordinate, then one face of the porphyrin is blocked and only one phenanthroline binds to the opposite face of the porphyrin. When the metalloporphyrin has two axial ligands, then no π–π complex is formed because both faces are sterically blocked.[29]

Formation of phenanthroline π–π complexes results in core-size and oxidation-state marker-line shifts similar to those observed upon aggregation. For example, complex induced shifts of 1–3 cm^{-1} for core-size marker lines are observed for complexes of unhindered 1,10-phenanthroline derivatives and isomers with Cu-, Ni-, and Fe(OH) uroporphyrins. Smaller increases in frequency of ν_4 are also observed.[9,26]

Another kind of π–π interaction is observed for complexes with molecules possessing not only extended π conjugation systems like phenanthroline but also charged substituent groups. For example, methyl viologen (4,4′-*N*-methylpyridinium dichloride) in solution has positively charged *N*-methyl groups at opposite ends of the molecule. As a result of electrostatic attraction, methyl viologen binds strongly to UroP with eight negatively charged carboxylates at the periphery of the porphyrin ring.[30] The electrostatic interaction apparently adds to the hydrophobic interaction and van der Waals forces that lead to complexation for neutral aromatic molecules like phenanthroline.

For the strong π–π complexes formed between uroporphyrins and viologens, a similar pattern of Raman marker-line shifts is observed for ν_4, ν_3, ν_{19}, and ν_{10}. Although the shifts in all of the marker lines are from 2 to 4 cm^{-1} for Cu(UroP), for example, decreases rather than increases in frequency are observed upon complex formation, in contrast with the aggregates and neutral π–π complexes.[30] A similar pattern of Raman marker-line shifts is found for viologen complexes with Ni-, Pd-, and Fe(OH) uroporphyrins in aqueous base.

Crystallizations. We observe that the crystallization experiments yielding crystals of the previously reported[4] triclinic A phase were, in our hands, only found when a small amount of the free base H_2OEP was also present in the crystallizing medium. We also observe that under our crystallization conditions H_2OEP is less soluble than Ni(OEP) and that the triclinic A phase is isomorphous with crystalline H_2OEP.[31] We conclude that it is likely that the triclinic A phase uses crystallites of H_2OEP as a template for crystallization of Ni(OEP). Thus, the presence of the free base promotes the formation of the triclinic A phase. It is also to be noted that the required impurity level of H_2OEP is quite low. Some years ago, we[32] noted that we could prepare much larger crystals of Co(TPP) if a small amount of free base H_2TPP was present in the crystallizing medium; in that case the free base was found to be incorporated in the crystalline "Co(TPP)".

Conclusions. The Raman results suggest that π–π interactions, in the crystalline phase B, cause a decrease in π charge density in the porphyrin ring. The decrease in π charge causes a contraction of the porphinato core. Evidence for the contraction is found in the comparison of the X-ray structures and in the differences in frequencies of the core-size marker lines for the two triclinic forms.

The direct observation in the X-ray structures of core contraction induced by π–π interaction in the crystal means that the small Raman shifts measured for the solution aggregates and complexes may be reliably interpreted in terms of changes in core size. Thus, for solution π–π aggregates and complexes a similar decrease in π charge is inferred from the marker-line shifts; a contraction of the central core about a central nickel ion is likely.

Acknowledgment. We thank the U.S. National Institutes of Health (Grant GM-38401 to W.R.S.), U.S. Department of Energy (Grant DE-AC04-76DP00789 to J.A.S.), and Gas Research Institute (Grant 5082-560-0767 to J.A.S.) for support of this research. We thank Dr. Charles Eigenbrot for assistance with the X-ray data collection.

Registry No. Ni(OEP), 24803-99-4.

Supplementary Material Available: Tables of anisotropic temperature factors (Table SI) and fixed hydrogen atom coordinates (Table SII) (2 pages); listing of observed and calculated structure amplitudes (×10) (9 pages). Ordering information is given on any current masthead page.

(24) Shelnutt, J. A.; Dobry, M. M. Satterlee, J. D. *J. Phys. Chem.* **1984**, *88*, 4980.
(25) Shelnutt, J. A. *J. Phys. Chem.* **1984**, *88*, 4988. Shelnutt, J. A.; Dobry, M. M. *J. Phys. Chem.* **1983**, *87*, 3012. Satterlee, J. D.; Shelnutt, J. A. *J. Phys. Chem.* **1984**, *88*, 5487. Satterlee, J. D.; Shelnutt, J. A. *Inorg. Chem. Acta* **1985**, *106*, 165.
(26) Shelnutt, J. A. *Inorg. Chem.* **1983**, *22*, 2535.
(27) Shelnutt, J. A.; Rosseau, D. L.; Dethmers, J. K.; Margoliash, E. *Biochemistry* **1981**, *20*, 6485. Adar, F. *Arch. Biochem. Biophys.* **1975**, *170*, 640. Adar, F. *Arch. Biochem. Biophys.* **1977**, *181*, 5.
(28) Shelnutt, J. A. *J. Am. Chem. Soc.* **1981**, *102*, 4275. Shelnutt, J. A. *J. Am. Chem. Soc.* **1983**, *105*, 774.
(29) Shelnutt, J. A. *J. Am. Chem. Soc.* **1983**, *105*, 7179. Shelnutt, J. A. U.S. Patent 4 568 435, 1986.
(30) Shelnutt, J. A. *J. Phys. Chem.* **1984**, *88*, 6121.
(31) Lauer, J. W.; Ibers, J. A. *J. Am. Chem. Soc.* **1973**, *95*, 5148.
(32) Madura, P.; Scheidt, W. R. *Inorg. Chem.* **1976**, *15*, 3182–3184.